

Spin-orbital entanglement in Cr^{3+} -doped glasses

J. S. Robles-Páez, A. T. Carreño-Santos, V. García-Rojas, and J. F. Pérez-Torres*
Escuela de Química, Universidad Industrial de Santander, Cra. 27-9, 680002 Bucaramanga, Colombia
(Dated: February 17, 2026)

A framework for reconstructing the one-electron spinors Γ_7 and Γ_8 of Cr^{3+} embedded in glasses from optical measurements has been developed. From the spinors, the spin-orbital von Neumann entropy can be calculated. An aluminum phosphate glass doped with 1 mol% chromium is prepared, and its optical absorption spectrum is recorded to validate the method. The spin-orbit coupling constant, crystal field strength, and Racah parameters are obtained from the absorption spectrum. Subsequently, the spin-orbital entanglement entropy is calculated and analyzed for a family of chromium-doped glasses. It is found that individually, neither the spin-orbit coupling constant, nor the crystal field strength, nor the Racah parameters correlate with the entanglement entropy. In contrast, the ratio between the spin-orbit coupling constant and the crystal field strength correlates linearly with the entanglement entropy.

I. INTRODUCTION

Quantum entanglement was originally conceived as a quantum mechanical phenomenon where two or more particles become so deeply linked that their quantum states can not be described independently, regardless of the distance separating them. This phenomenon has been observed in several scenarios using photons [1, 2], electrons [3] and calcium monofluoride molecules [4]. The concept of entanglement can be extended to other scenarios that transcend its mathematical definition, which states that maximum knowledge about the whole of a system does not imply maximum knowledge about the individual parts of that system. With the parts of the system, one can consider the degrees of freedom. Thus, for example, nowadays we can refer to the entanglement between the spin angular momentum and the orbital angular momentum of a single electron within an atom, molecule or solid [5–8]. Among the systems which can exhibit spin-orbital entanglement, are the transition metal ions, in particular with an odd number of electrons. This entanglement drives the magnetic properties of the 4d and 5d transition metals [5], in which the spin-orbit coupling strength is appreciable. Nonetheless, some 3d systems can exhibit this entanglement in very specific situations. The importance of spin-orbital interaction in transition metal-halide perovskites has been recently identified [9]. Among the compounds with 3d transition metal ions that display spin-orbital entanglement are Cr^{3+} -doped glasses. In such systems, spin-orbital interaction manifests itself in the visible absorption spectrum, where one or two absorption bands show an interference pattern. The optical absorption spectrum of transition metal ions embedded in a glass can be explained in terms of the crystal field theory. For example, in a Cr^{3+} -doped phosphate glass, the chromium(III) is surrounded by six oxygen ions in octahedral symmetry, see Figure 1. In this case, the crystal field theory predicts the 3d atomic orbitals split

into t_{2g} and e_g crystal field orbitals. Then, the three electrons accommodate in the six lowest energy spin-orbitals $t_{2g} \otimes (\alpha \cup \beta)$, electron configuration t_{2g}^3 , giving rise to multiplets ${}^4\text{A}_2$, ${}^2\text{E}$, ${}^2\text{T}_1$ and ${}^2\text{T}_2$. According to the first Hund's rule, the multiplet ${}^4\text{A}_2$ is the ground state. When an electron jump to one of the four high energy spin-orbitals $e_g \otimes (\alpha \cup \beta)$, it yields the electron configuration $t_{2g}^2 e_g^1$ and the multiplets ${}^2\text{A}_1$, ${}^2\text{A}_2$, ${}^2\text{E}$, ${}^4\text{T}_1$, and ${}^4\text{T}_2$ are formed. Because the spin selection rule, only the transitions ${}^4\text{T}_2 \leftarrow {}^4\text{A}_2$ and ${}^4\text{T}_1 \leftarrow {}^4\text{A}_2$ are expected to be observed, accounting for the absorption bands. However, as stated before, the absorption bands of Cr^{3+} -doped glasses show interference patterns. Bussière et al. [10] and Maalej et al. [11] have managed not only to explain the interference pattern in terms of the interaction between the doublets ${}^2\text{E}$, ${}^2\text{T}_1$, and ${}^2\text{T}_2$ with the quadruplets ${}^4\text{T}_2$ and ${}^4\text{T}_1$, but also to extract the one-electron spin-orbit coupling constant from the pattern based on a method developed by Neuhauser et al. [12]. In this work, we employ a framework based on the relativistic crystal field theory [13] and Neuhauser's method [12] to quantify the spin-orbital entanglement in Cr^{3+} -doped glasses. The standard measurement of entanglement is the entanglement entropy [14–17]. We prove that for Cr^{3+} -doped glasses, and in general for Cr^{3+} systems exhibiting interference patterns in the absorption spectrum, the spin-orbital entanglement entropy can be calculated from the optical absorption spectrum. The spin-orbit coupling interaction and the corresponding interference pattern have been analysed in Cr^{3+} -doped fluoride [11] and tellurite [18] glasses. To increase the variety of glasses, we also prepare a Cr^{3+} -doped aluminum phosphate glass and calculate the spin-orbital entanglement from the interference pattern appearing in the absorption spectrum. The remainder of this paper is organized as follows: In Section 2 the crystal field theory and its relativistic version is briefly described together with the Neuhauser et al. [12] and Bussière et al. [10] method to extract the one-electron spin-orbit coupling constant. In Section 3 the preparation of the chromium-doped aluminum phosphate glass is described. In Section 4 the results are presented, comprising the calculation and the analysis

* jfperez@uis.edu.co

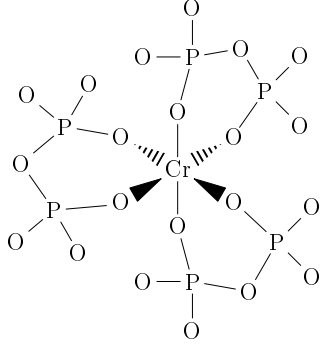


FIG. 1. Idealized octahedral structure of CrO_6 in phosphate glasses.

of the spin-orbital entanglement entropy. Finally, some conclusions are outlined in Section 5.

II. THEORETICAL FRAMEWORK

A. Crystal field theory

The crystal field theory, established in the early of the past century mainly by H. Bethe [19] and J. H. van Vleck [20], describes the optical and magnetic properties of d^n transition metal atoms surrounded by N point charges named as ligands in a specific configuration. In its standard version, perturbation theory is used to obtain the eigenvalues and eigenvectors of the crystal field CF Hamiltonian

$$\mathcal{H}_{\text{CF}} = \alpha \hbar c \sum_{i=1}^N \frac{Z}{|\mathbf{r} - \mathbf{R}_i|} \quad (1)$$

in the basis of atomic d-orbitals $|n\ell m\rangle$. Here, α is the fine structure constant, \hbar is the reduced Planck constant, c is the velocity of the light in vacuum, Z is the effective charge of the ligands, \mathbf{r} is the position of the electron, and \mathbf{R}_i is the position of each ligand. For six coordinated transition metal ions, the octahedral crystal field yields the following eigenvectors [21]

$$|t_{2g}^-\rangle = |nd_{-1}\rangle \quad (2)$$

$$|t_{2g}^+\rangle = |nd_{+1}\rangle \quad (3)$$

$$|t_{2g}^0\rangle = \frac{1}{\sqrt{2}} (|nd_{-2}\rangle - |nd_{+2}\rangle) \quad (4)$$

$$|e_g^a\rangle = \frac{1}{\sqrt{2}} (|nd_{-2}\rangle + |nd_{+2}\rangle) \quad (5)$$

$$|e_g^b\rangle = |nd_0\rangle \quad (6)$$

and eigenvalues

$$E(e_g) = 6Dq \quad (7)$$

$$E(t_{2g}) = -4Dq \quad (8)$$

where Dq is the crystal field strength defined by

$$Dq = \alpha \hbar c \frac{Z}{6a} \int_0^\infty |f_{nd}(r)|^2 r^4 dr \quad (9)$$

where a stands for the ligand-metal distance. The function $f_{nd}(r)$ is the radial part of the d-atomic orbitals $\psi_{ndm}(r) = f_{nd}(r)Y_{2m}(\theta\phi)/r$ with $Y_{2m}(\theta\phi)$ the spherical harmonics of $\ell = 2$. In the relativistic version of the crystal field theory [13, 22], the eigenvectors of the total Hamiltonian $\mathcal{H} = c\hat{\mathbf{a}} \cdot \hat{\mathbf{p}} + \beta m_e c^2 + V(r) + \mathcal{H}_{\text{CF}}$ are obtained in the basis of atomic Dirac d-spinors $|n\kappa m_j\rangle$,

$$|\Gamma_{8\pm}^a\rangle = x_\pm \left(\sqrt{\frac{5}{6}}|n-3-\frac{5}{2}\rangle + \sqrt{\frac{1}{6}}|n-3+\frac{3}{2}\rangle \right) + y_\pm |n+2+\frac{3}{2}\rangle \quad (10)$$

$$|\Gamma_{8\pm}^b\rangle = x_\pm \left(\sqrt{\frac{5}{6}}|n-3+\frac{5}{2}\rangle + \sqrt{\frac{1}{6}}|n-3-\frac{3}{2}\rangle \right) - y_\pm |n+2-\frac{3}{2}\rangle \quad (11)$$

$$|\Gamma_{8\pm}^c\rangle = x_\pm |n-3-\frac{1}{2}\rangle + y_\pm |n+2-\frac{1}{2}\rangle \quad (12)$$

$$|\Gamma_{8\pm}^d\rangle = x_\pm |n-3+\frac{1}{2}\rangle - y_\pm |n+2+\frac{1}{2}\rangle \quad (13)$$

$$|\Gamma_7^a\rangle = \sqrt{\frac{1}{6}}|n-3-\frac{5}{2}\rangle - \sqrt{\frac{5}{6}}|n-3+\frac{3}{2}\rangle \quad (14)$$

$$|\Gamma_7^b\rangle = \sqrt{\frac{1}{6}}|n-3+\frac{5}{2}\rangle - \sqrt{\frac{5}{6}}|n-3-\frac{3}{2}\rangle \quad (15)$$

with

$$x_\pm = \frac{\delta \pm \sqrt{\delta^2 + 1}}{\sqrt{(\delta \pm \sqrt{\delta^2 + 1})^2 + 1}} \quad (16)$$

$$y_\pm = \frac{1}{\sqrt{(\delta \pm \sqrt{\delta^2 + 1})^2 + 1}} \quad (17)$$

$$\delta = \frac{1}{2\sqrt{6}(p/q)} \left(\frac{5\xi_{nd}}{4Dq} + 1 \right) \quad (18)$$

$$\xi_{nd} = \frac{2}{5} (E(nd_{5/2}) - E(nd_{3/2})) \quad (19)$$

$$Dq = \alpha \hbar c \frac{Z}{6a} \int_0^\infty |F_{nd_{5/2}}(r)|^2 r^4 dr \quad (20)$$

$$p/q = \frac{\int_0^\infty F_{nd_{5/2}}(r) F_{nd_{3/2}}(r) r^4 dr}{\int_0^\infty |F_{nd_{5/2}}(r)|^2 r^4 dr} \quad (21)$$

and eigenvalues

$$E(\Gamma_{8\pm}) = Dq - \frac{\xi_{nd}}{4} \pm Dq \sqrt{\left(\frac{5\xi_{nd}}{4Dq} + 1 \right)^2 + 24(p/q)^2} \quad (22)$$

$$E(\Gamma_7) = \xi_{nd} - 4Dq \quad (23)$$

where ξ_{nd} stands for the spin-orbit coupling constant. In the non relativistic limit, the radial functions of the d-spinors $F_{nd_{3/2}}(r)$ and $F_{nd_{5/2}}(r)$ are both equal to the radial function of the d-orbitals $f_{nd}(r)$. In such case one

obtains $p/q = 1$, $\xi_{nd} = 0$, $E(\Gamma_{8-}) = E(\Gamma_7) = E(t_{2g})$, and $E(\Gamma_{8+}) = E(e_g)$, i.e. the standard crystal field theory is re-established, see Fig. 2. The relativistic crystal field theory is particularly preferred when the spin-orbit interaction is observed, and fundamental in the description of the 5d transition metal ions where the spin-orbit interaction can not be neglected [13, 22]. Notice that,

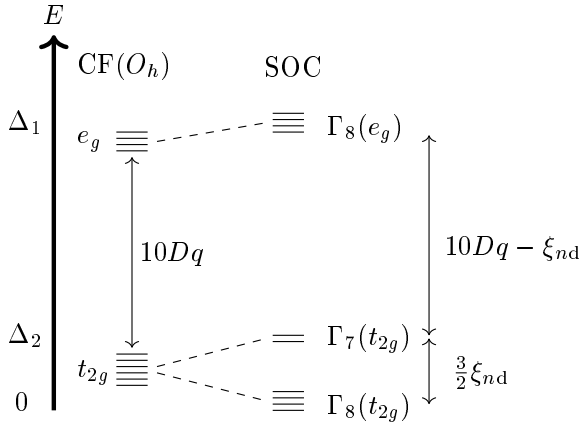


FIG. 2. Energy splitting of d orbitals due to octahedral crystal field $CF(O_h)$ and to the spin-orbit coupling SOC.

unlike the crystal field orbitals t_{2g} and e_g , the relativistic crystal field spinors Γ_i depend not only on the spin-orbit coupling constant ξ_{nd} , as would be expected, but also on the crystal field parameter Dq and on the relativistic ratio p/q . We have recently developed a formalism to quantify the spin-orbital entanglement characteristic of the spinors using the von Neumann entropy [23],

$$S_{vN}(\Gamma_i) = -\lambda(\Gamma_i) \log_2(\lambda(\Gamma_i)) - (1 - \lambda(\Gamma_i)) \log_2(1 - \lambda(\Gamma_i)) \quad (24)$$

with

$$\lambda(\Gamma_7^{ab}) = \frac{2}{3} \quad (25)$$

$$\lambda(\Gamma_{8\pm}^{ab}) = \frac{2}{15}x_{\pm}^2 + \frac{1}{5}y_{\pm}^2 - \frac{2\sqrt{6}}{15}x_{\pm}y_{\pm} \quad (26)$$

$$\lambda(\Gamma_{8\pm}^{cd}) = \frac{2}{5}x_{\pm}^2 + \frac{3}{5}y_{\pm}^2 - \frac{2\sqrt{6}}{5}x_{\pm}y_{\pm} \quad (27)$$

Due to the symmetry restrictions on the wave function imposed by the double point group O_h^* [24], the spin-orbit entanglement entropy has to be redefined as

$$\Delta S_{vN}^{SO}(\Gamma_i) = S_{vN}(\Gamma_i) - S_{vN}^{(\xi_{nd}=0)}(\Gamma_i) \quad (28)$$

However, only spinors $\Gamma_8^{ab}(t_{2g})$ and $\Gamma_7^{ab}(t_{2g})$ are affected by the term $S_{vN}^{(\xi_{nd}=0)}$ [23]. The defined von Neumann entropies quantifies the spin-orbital entanglement, not present in the orbitals of the standard crystal field theory. We remind the reader that a state is entangled if it can not be written as a separable state, i.e. $|\Gamma_i\rangle \neq |n\ell m\rangle \otimes |sm_s\rangle$. For 3d ions, the relativistic ratio can be approximated to one, $p/q = 1$. Therefore, only the crystal field strength Dq and the spin-orbit coupling constant ξ_{nd} are needed to calculate the corresponding entropies.

B. Determination of the crystal field parameters

In this section we describe how to obtain, from the optical absorption spectrum, the Racah parameters B and C , the crystal field strength Dq , and the spin-orbit coupling constant ξ_{3d} . Nevertheless, only Dq and ξ_{3d} are needed to calculate the spin-orbital entanglement entropies. For a 3d³ ion in octahedral field, the crystal field strength Dq and the Racah parameter B can be straightforwardly obtained by [25]

$$Dq = \frac{E(^4T_2)}{10} \quad (29)$$

$$B = \frac{(E(^4T_1) - 2E(^4T_2))(E(^4T_1) - E(^4T_2))}{15E(^4T_1) - 27E(^4T_2)} \quad (30)$$

while the second Racah parameter C is obtained by varying it in the interaction matrix [26]

$$\begin{pmatrix} -12Dq - 6B + 3C & -6\sqrt{2}B & -3\sqrt{2}B & 0 \\ -6\sqrt{2}B & -2Dq + 8B + 7C & 10B & \sqrt{3}(2B + C) \\ -3\sqrt{2}B & 10B & -2Dq - B + 3C & 2\sqrt{3}B \\ 0 & \sqrt{3}(2B + C) & 2\sqrt{3}B & 18Dq - 8B + 4C \end{pmatrix} \quad (31)$$

until the lowest eigenvalue coincides with the observed energy $E(^2E)$. When the 2E and 2T_1 states interact with the 4T_1 state through the spin-orbit coupling, the optical

band $^4T_1 \leftarrow ^4A_2$ exhibits one or two interference dips. This interference is frequently observed in d³ chromium and 3d⁸ nickel ions [10, 11, 27, 28], and can be used to

estimate an effective spin-orbit coupling constant. Following the framework developed by Neuhauser et al. [12] and Bussière et al. [10], the one-electron spin-orbit coupling constant [11], $\xi_{3d} = \sqrt{5/6}\gamma_1$, is obtained by fitting the parameters γ_1 , γ_2 , Γ_0 , Γ_1 and Γ_2 of the line shape function $\sigma(\omega)$

$$\sigma(\omega) = -\frac{1}{\pi} \text{Im} \left(\frac{\beta}{1 - (\alpha_1 \gamma_1^2 + \alpha_2 \gamma_2^2) \beta} \right) \quad (32)$$

$$\alpha_i = \frac{1}{\omega - \epsilon_i + i\Gamma_i}, \quad i = 1, 2 \quad (33)$$

$$\beta = \frac{1}{\omega - 10Dq + i\Gamma_0} \quad (34)$$

to the experimental optical absorption spectrum. This is achieved by minimizing the integral

$$I(\Gamma_1, \Gamma_2, \gamma_1, \gamma_2) = \int_{\omega_1}^{\omega_2} [\sigma(\omega, \Gamma_1, \Gamma_2, \gamma_1, \gamma_2) - \sigma_{\text{exp}}(\omega)]^2 d\omega \quad (35)$$

Here, ω is the photon energy, ϵ_1 and γ_1 are the energy at the dip and the coupling constant between states 2E and 4T_2 , respectively; ϵ_2 and γ_2 are the energy at the dip and the coupling constant between states 4T_2 and 2T_1 , respectively; Γ_0 , Γ_1 and Γ_2 are damping factors that determine the width of individual vibronic lines of the spin allowed Γ_0 and spin forbidden Γ_1 and Γ_2 transitions, respectively. For more details on the parameters γ_i and Γ_i reader can consult Refs. [10, 11]. We should also highlight that the effective spin-orbit coupling which mixes the crystal field orbitals t_{2g} and e_g [29], can also be experimentally probed by X-ray Absorption Spectroscopy (XAS) measurements.

III. PREPARATION OF THE GLASS SYSTEM

Conventional melt-quenching technique was used to prepare aluminum phosphate glass with $50\text{P}_2\text{O}_5\text{-}44\text{Na}_2\text{O}\text{-}5\text{Al}_2\text{O}_3\text{-Cr}$ composition using as raw materials reagent grade Al_2O_3 (neutral, chromatography grade, Carlo Elba), Na_2CO_3 ($\geq 99.9\%$, Sigma-Aldrich) and $\text{NH}_4\text{H}_2\text{PO}_4$ ($\geq 98\%$, Sigma-Aldrich). The choice of tris(acetylacetone)chromium(III), $\text{Cr}(\text{acac})_3$, as a precursor of chromium occurs because it enables working in a system free from chlorides, thereby not allowing any alteration in the composition of the glass, and due to its high chemical stability which favors the incorporation of chromium exclusively in the Cr^{3+} oxidation state. $\text{Cr}(\text{acac})_3$ was synthesized according to the procedure reported by Fernelius et al. [30] using $\text{CrCl}_3 \cdot 6\text{H}_2\text{O}$ ($\geq 99\%$, J. T. Baker) and acetylacetone ($\geq 99\%$, Sigma-Aldrich) on an Anton Paar monowave 400 microwave synthesis reactor. Appropriate quantities of the compounds were weighed, mixed, ground in an agate mortar and melted in porcelain crucibles under air atmosphere using an electric furnace programmed to increase the temperature at $10\text{ }^{\circ}\text{C}/\text{min}$ from room temperature to $950\text{ }^{\circ}\text{C}$

and maintained at this temperature for 1 hour. Rate of $10\text{ }^{\circ}\text{C}/\text{min}$ was used in order to eliminate water, ammonia and acac^- . The melt was poured rapidly onto a preheated graphite mold at $350\text{ }^{\circ}\text{C}$ and then cold down to room temperature. The fabricated glass piece was weighed and found to be 1.867 g. The absorption spectrum was recorded using a Genesys 50 UV-Vis spectrometer (Thermo Fisher Scientific).

IV. RESULTS

Figure 3 shows the experimental and fitted optical absorption spectrum of the aluminum phosphate glass doped with 1 mol % Cr^{3+} . The energy correlation diagram for the d^3 ions is also shown. This type of Tanabe-Sugano energy-level diagram is widely used in coordination chemistry for a fundamental understanding of the interplay between electron-electron repulsion and crystal field strength [26, 31, 32]. The absorption spectrum exhibits two depressions within the first absorption band centered at 15256 cm^{-1} ($\lambda = 655.5\text{ nm}$) and a shoulder within the second absorption band centered at 22148 cm^{-1} ($\lambda = 451.5\text{ nm}$). From these results, we obtain a crystal field strength of $Dq = 1526\text{ cm}^{-1}$, and Racah parameters $B = 723\text{ cm}^{-1}$ and $C = 3108\text{ cm}^{-1}$. The ratio $Dq/(Dq + B) = 0.683$, marked with a rectangle in the correlation diagram (Fig. 3), confirms the participation of the spin-forbidden states 2E , 2T_1 , and 2T_2 in the absorption spectrum. The fitting parameters, $\Gamma_1 = 240\text{ cm}^{-1}$, $\Gamma_2 = 180\text{ cm}^{-1}$, $\gamma_1 = 250\text{ cm}^{-1}$, and $\gamma_2 = 190\text{ cm}^{-1}$, result in a one-electron spin-orbit coupling constant of $\xi_{3d} = 228\text{ cm}^{-1}$. After calculating ξ_{3d}

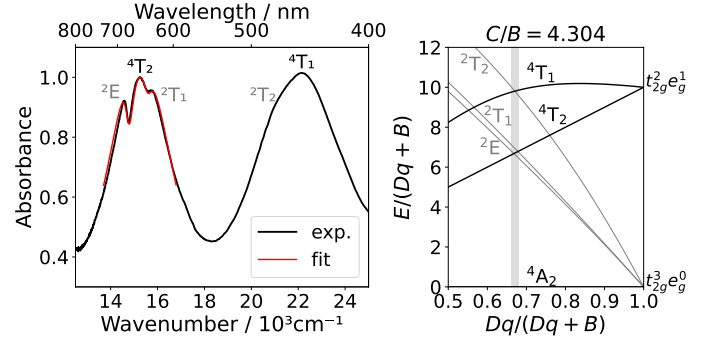


FIG. 3. Left: absorption spectrum of 1 mol % Cr^{3+} doped phosphate glass. The fitted spectrum correspond to the parameters $\Gamma_0 = 1850\text{ cm}^{-1}$, $\Gamma_1 = 240\text{ cm}^{-1}$, $\Gamma_2 = 180\text{ cm}^{-1}$, $\gamma_1 = 250\text{ cm}^{-1}$, and $\gamma_2 = 190\text{ cm}^{-1}$. Right: Correlation diagram of energy levels of d^3 ions as a function of $Dq/(Dq + B)$. The rectangle indicates the Cr^{3+} -doped phosphate glass absorption bands.

and Dq , we proceed to calculate the amplitudes of the one-electron spinors and the corresponding entanglement entropies. Using $\xi_{3d} = 228\text{ cm}^{-1}$, $Dq = 1526\text{ cm}^{-1}$, and $p/q = 1$, we obtain $\delta = 0.242$ which yields $x_- = -y_+ = -0.618$ and $y_- = x_+ = 0.786$. These amplitudes reveal

TABLE I. Spin-orbit coupling constants, crystal field parameters, and spin-orbital entanglement entropies for a family of Cr^{3+} -doped glasses. ZLAG, ZBLA and PZG comprise fluoride glasses [11]; PT, CT and ZT comprise tellurite glasses with composition $\text{ZnF}_2\text{-RO-TeO}_2$ (R = Pb, Cd and Zn) [18]; AlPO refers to aluminum-doped phosphate glass.

Glass system	ξ_{3d}/cm^{-1}	Dq/cm^{-1}	Dq/B	C/B	$\Delta S_{\text{vN}}^{\text{SO}}$		
					$\Gamma_8^{ab}(t_{2g})$	$\Gamma_8^{ab}(e_g)$	$\Gamma_8^{cd}(t_{2g}, e_g)$
ZLAG Ref. [11]	209	1441	1.81	3.95	-0.000104	0.001520	0.004069
ZBLA Ref. [11]	213	1482	1.82	3.76	-0.000102	0.001496	0.004004
PZG Ref. [11]	218	1502	1.97	4.07	-0.000104	0.001522	0.004074
AlPO (this work)	228	1526	2.11	4.30	-0.000111	0.001603	0.004288
PT Ref. [18]	240	1489	1.93	3.53	-0.000128	0.001836	0.004900
CT Ref. [18]	241	1497	1.92	3.52	-0.000128	0.001832	0.004890
ZT Ref. [18]	241	1505	1.91	3.44	-0.000126	0.001815	0.004844

a strong mixing of the atomic spinors $3d_{3/2}$ and $3d_{5/2}$. This is because in $3d^n$ systems, the spin-orbit interaction is small compared to the strength of the crystal field; therefore, the crystal field spinors are mixed to represent the crystal field spin-orbitals, which ultimately turn out to be a reasonable, albeit non-entangled, basis. The entanglement entropies are presented in Table I, which also includes the spin-orbit coupling constant and the crystal field parameters for a family of chromium-doped glasses. The Neuhauser's parameters obtained from the optical absorption spectra of fluoride [11] and tellurite glasses [18] doped with Cr^{3+} will be used for the theoretical study in this article. The molar composition of fluoride glasses are [11]: ZLAG(70.2 ZrF_4 , 23.4 LaF_3 , 0.6 AlF_3 , 5.8 GaF_3 , 0.5 CrF_3), ZBL(57 ZrF_4 , 5 LaF_3 , 3.5 AlF_3 , 34 BaF_2 , 0.5 CrF_3), and PZG(2 AlF_3 , 34.3 GaF_3 , 35.3 PbF_2 , 4.9 YF_3 , 23.5 ZnF_2 , 0.5 CrF_3); while

the tellurite glasses are made of [18, 33] $\text{ZnF}_2\text{-MO-TeO}_2$ with MO=Pb labeled as PT, MO=CdO labeled as CT, and MO=ZnO labeled as ZT, and the Cr^{3+} content was varied from 0.1 % to 0.3 %. We observe that the entanglement entropy does not correlate with any of the Racah or crystal field strength parameters. On the other hand, the spin-orbit coupling constant generally appears to correlate with the entanglement entropy, except in the case of tellurite glasses, where the differences are small, if not negligible. In a previous work, we had found that entanglement entropy correlates well with the effective magnetic dipole moment in a family of $5d^1$ transition metal perovskites and hexachlorides [23]. Nevertheless, a correlation between the ξ_{3d}/Dq ratio and the entanglement entropy mediated by the parameter δ is expected, see Eq (18).

Figure 4 shows the entanglement entropy $\Delta S_{\text{vN}}^{\text{SO}}(\Gamma_8^{cd}(t_{2g}, e_g))$ versus ξ_{3d}/Dq for the glasses analysed here. A linear correlation can be observed. This can be explained as follows: since we are dealing with a $3d$ transition metal ion, the strong field approximation $\xi_{nd}/10Dq \gg 1$ is valid. Therefore, the one-electron spinors can be expressed in terms of the standard crystal field spin-orbitals $(t_{2g} \cup e_g) \otimes (\alpha \cup \beta)$ (see Appendix). Indeed, when the crystal field spinors are rewritten in terms of the crystal field spin-orbitals, it is found that the contribution of the crystal field orbital e_g to the ground state, $(\sqrt{15}x_- + \sqrt{10}y_-)^2/25$, barely reaches 0.03 %. Therefore, the ground state multiplet ${}^4\text{A}_{2g}$ is perfectly represented by the configuration t_{2g}^3 , from which the spin-only formula for the magnetic dipole moment is expected to be valid. This is consistent with the magnitude of the entanglement entropy found here, which turns out to be two orders of magnitude smaller than those obtained for the double perovskites $\text{Ba}_2\text{MgReO}_6$ and $\text{Ba}_2\text{NaOsO}_6$, whose entropies $\Delta S_{\text{vN}}^{\text{SO}}(\Gamma_8^{cd}(t_{2g}, e_g))$ are 0.2112 and 0.2094,

respectively [23]. From Figure 4 we also observe that entanglement entropy serves as a descriptor of the nature of the host, i.e., it classifies glasses into families: tellurite glasses with the highest entropy, followed by phosphate glass, and then fluoride glasses with the lowest entropy.

V. CONCLUSION

In conclusion, we have developed and implemented a framework to quantify spin-orbital entanglement in one-electron spinors of Cr^{3+} embedded in glasses. The framework is based on relativistic crystal field theory [13] and Neuhauser's method for extracting the one-electron spin-orbit coupling constant from the absorption spectrum [12]. The developed framework is timely taking into account the recent interest in detecting spin-orbital entanglement [8, 34]. The ratio between the spin-orbital coupling constant and the strength of the crystal field ξ_{3d}/Dq turns out to be a criterion for discerning the chemical nature of the host glass. This is reinforced by the linear

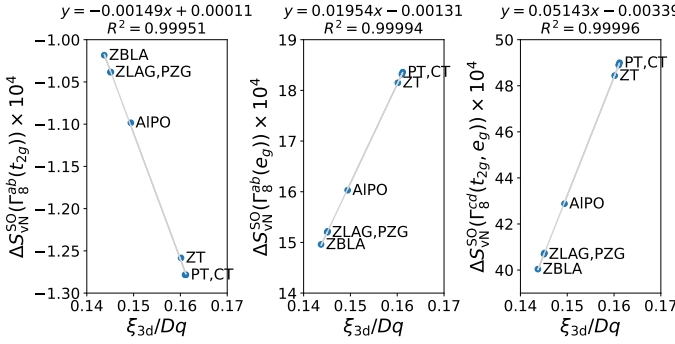


FIG. 4. Spin-orbital entanglement entropy of Γ_8 espinors of Cr^{3+} -doped glasses versus ξ_{3d}/Dq ratio. ZLAG, ZBLA and PZG stand for fluoride glasses; PT, CT, and ZT stand for tellurite glasses; AIPO stands for aluminum-phosphate glass.

relationship existing between the ratio ξ_{3d}/Dq and the spin-orbital entanglement entropy $\Delta S_{vN}^{\text{SO}}(\Gamma_i)$ when the

strong field approximation is valid. It would be interesting to extent the analysis of the spin-orbital entanglement not only to other types of Cr^{3+} -doped glasses, but also to other materials. Work along this line is currently in progress.

Appendix A: Basis transformations

The crystal field orbitals mix in order to recover the atomic orbitals according to

$$\begin{bmatrix} |nd_{-2}\rangle \\ |nd_{-1}\rangle \\ |nd_0\rangle \\ |nd_{+1}\rangle \\ |nd_{+2}\rangle \end{bmatrix} = \begin{bmatrix} 0 & \frac{\sqrt{2}}{2} & 0 & \frac{\sqrt{2}}{2} & 0 \\ 1 & 0 & 0 & 0 & 0 \\ 0 & 0 & 0 & 0 & 1 \\ 0 & 0 & 1 & 0 & 0 \\ 0 & -\frac{\sqrt{2}}{2} & 0 & \frac{\sqrt{2}}{2} & 0 \end{bmatrix} \begin{bmatrix} |t_{2g}^-\rangle \\ |t_{2g}^0\rangle \\ |t_{2g}^+\rangle \\ |e_g^a\rangle \\ |e_g^b\rangle \end{bmatrix} \quad (\text{A1})$$

Assuming $F_{nd_{5/2}}(r) = F_{nd_{3/2}}(r)$, where $F_{nd_j}(r)$ is the radial part of the large component of the atomic spinors [35], the atomic spinors can be written in terms of the atomic spin-orbitals:

$$\begin{bmatrix} |n2-\frac{3}{2}\rangle \\ |n2-\frac{1}{2}\rangle \\ |n2+\frac{1}{2}\rangle \\ |n2+\frac{3}{2}\rangle \\ |n-3+\frac{5}{2}\rangle \\ |n-3-\frac{5}{2}\rangle \\ |n-3-\frac{3}{2}\rangle \\ |n-3-\frac{1}{2}\rangle \\ |n-3+\frac{1}{2}\rangle \\ |n-3+\frac{3}{2}\rangle \end{bmatrix} = \begin{bmatrix} -\frac{2\sqrt{5}}{5} & 0 & 0 & 0 & 0 & \frac{\sqrt{5}}{5} & 0 & 0 & 0 \\ 0 & -\frac{\sqrt{15}}{5} & 0 & 0 & 0 & 0 & \frac{\sqrt{10}}{5} & 0 & 0 \\ 0 & 0 & -\frac{\sqrt{10}}{5} & 0 & 0 & 0 & 0 & \frac{\sqrt{15}}{5} & 0 \\ 0 & 0 & 0 & -\frac{\sqrt{5}}{5} & 0 & 0 & 0 & 0 & \frac{2\sqrt{5}}{5} \\ 0 & 0 & 0 & 0 & 1 & 0 & 0 & 0 & 0 \\ 0 & 0 & 0 & 0 & 0 & 1 & 0 & 0 & 0 \\ \frac{\sqrt{5}}{5} & 0 & 0 & 0 & 0 & 0 & \frac{2\sqrt{5}}{5} & 0 & 0 \\ 0 & \frac{\sqrt{10}}{5} & 0 & 0 & 0 & 0 & 0 & \frac{\sqrt{15}}{5} & 0 \\ 0 & 0 & \frac{\sqrt{15}}{5} & 0 & 0 & 0 & 0 & 0 & \frac{\sqrt{10}}{5} \\ 0 & 0 & 0 & \frac{2\sqrt{5}}{5} & 0 & 0 & 0 & 0 & \frac{\sqrt{5}}{5} \end{bmatrix} \begin{bmatrix} |nd_{-2}\alpha\rangle \\ |nd_{-1}\alpha\rangle \\ |nd_0\alpha\rangle \\ |nd_{+1}\alpha\rangle \\ |nd_{+2}\alpha\rangle \\ |nd_{-2}\beta\rangle \\ |nd_{-1}\beta\rangle \\ |nd_0\beta\rangle \\ |nd_{+1}\beta\rangle \\ |nd_{+2}\beta\rangle \end{bmatrix} \quad (\text{A2})$$

Then, the crystal field spinors,

$$\begin{bmatrix} |\Gamma_{8\pm}^a\rangle \\ |\Gamma_{8\pm}^b\rangle \\ |\Gamma_{8\pm}^c\rangle \\ |\Gamma_{8\pm}^d\rangle \\ |\Gamma_7^a\rangle \\ |\Gamma_7^b\rangle \end{bmatrix} = \begin{bmatrix} 0 & 0 & 0 & y & 0 & \frac{\sqrt{30}x_{\pm}}{6} & 0 & 0 & 0 & \frac{\sqrt{6}x_{\pm}}{6} \\ -y_{\pm} & 0 & 0 & 0 & 0 & \frac{\sqrt{30}x_{\pm}}{6} & 0 & \frac{\sqrt{6}x_{\pm}}{6} & 0 & 0 \\ 0 & y_{\pm} & 0 & 0 & 0 & 0 & 0 & x_{\pm} & 0 & 0 \\ 0 & 0 & -y_{\pm} & 0 & 0 & 0 & 0 & 0 & x_{\pm} & 0 \\ 0 & 0 & 0 & 0 & 0 & \frac{\sqrt{6}}{6} & 0 & 0 & 0 & -\frac{\sqrt{30}}{6} \\ 0 & 0 & 0 & 0 & 0 & \frac{\sqrt{6}}{6} & 0 & -\frac{\sqrt{30}}{6} & 0 & 0 \end{bmatrix} \begin{bmatrix} |n2-\frac{3}{2}\rangle \\ |n2-\frac{1}{2}\rangle \\ |n2+\frac{1}{2}\rangle \\ |n2+\frac{3}{2}\rangle \\ |n-3+\frac{5}{2}\rangle \\ |n-3-\frac{5}{2}\rangle \\ |n-3-\frac{3}{2}\rangle \\ |n-3-\frac{1}{2}\rangle \\ |n-3+\frac{1}{2}\rangle \\ |n-3+\frac{3}{2}\rangle \end{bmatrix} \quad (\text{A3})$$

can be written in terms of the crystal field spin-orbitals:

$$|\Gamma_{8\pm}^a\rangle = \left(\frac{\sqrt{30}x_{\pm}}{15} - \frac{\sqrt{5}y_{\pm}}{5} \right) |t_{2g}^+ \alpha\rangle + \left(\frac{2\sqrt{15}x_{\pm}}{15} - \frac{\sqrt{10}y_{\pm}}{5} \right) |t_{2g}^0 \beta\rangle + \left(\frac{\sqrt{15}x_{\pm}}{5} + \frac{\sqrt{10}y_{\pm}}{5} \right) |e_g^a \beta\rangle \quad (\text{A4})$$

$$|\Gamma_{8\pm}^b\rangle = \left(\frac{\sqrt{30}x_{\pm}}{15} - \frac{\sqrt{5}y_{\pm}}{5} \right) |t_{2g}^- \beta\rangle - \left(\frac{2\sqrt{15}x_{\pm}}{15} - \frac{\sqrt{10}y_{\pm}}{5} \right) |t_{2g}^0 \alpha\rangle + \left(\frac{\sqrt{15}x_{\pm}}{5} + \frac{\sqrt{10}y_{\pm}}{5} \right) |e_g^a \alpha\rangle \quad (\text{A5})$$

$$|\Gamma_{8\pm}^c\rangle = \left(\frac{\sqrt{10}x_{\pm}}{5} - \frac{\sqrt{15}y_{\pm}}{5} \right) |t_{2g}^- \alpha\rangle + \left(\frac{\sqrt{15}x_{\pm}}{5} + \frac{\sqrt{10}y_{\pm}}{5} \right) |e_g^b \beta\rangle \quad (\text{A6})$$

$$|\Gamma_{8\pm}^d\rangle = \left(\frac{\sqrt{10}x_{\pm}}{5} - \frac{\sqrt{15}y_{\pm}}{5} \right) |t_{2g}^+ \beta\rangle + \left(\frac{\sqrt{15}x_{\pm}}{5} + \frac{\sqrt{10}y_{\pm}}{5} \right) |e_g^b \alpha\rangle \quad (\text{A7})$$

$$|\Gamma_7^a\rangle = -\frac{\sqrt{6}}{3} |t_{2g}^+ \alpha\rangle + \frac{\sqrt{3}}{3} |t_{2g}^0 \beta\rangle \quad (\text{A8})$$

$$|\Gamma_7^b\rangle = -\frac{\sqrt{6}}{3} |t_{2g}^- \beta\rangle - \frac{\sqrt{3}}{3} |t_{2g}^0 \alpha\rangle \quad (\text{A9})$$

ACKNOWLEDGMENTS

There is no funding to report in this work. J. S. Robles-Páez and A. T. Carreño-Santos prepared the chromium-doped phosphate glass. J. F. Pérez-Torres conceived the original idea, developed the theoretical framework, and performed the calculations. V. García-Rojas acquired the resources and was in charge of the project. All the authors discussed the results and contributed to the final manuscript.

DATA AVAILABILITY

All the numerical results shown in this work can be obtained from the formulas and parameters described in the text. The optical absorption spectrum of aluminum-phosphate doped-chromium glass is available from the corresponding author upon reasonable request.

[1] S. J. Freedman and J. F. Clauser, Experimental test of local hidden-variable theories, *Phys. Rev. Lett.* **28**, 938 (1972).

[2] A. Aspect, P. Grangier, and G. Roger, Experimental Realization of Einstein-Podolsky-Rosen-Bohm Gedanken-experiment: A New Violation of Bell's Inequalities, *Phys. Rev. Lett.* **49**, 91 (1982).

[3] B. Hensen, H. Bernien, A. E. Dréau, A. Reiserer, N. Kalb, M. S. Blok, J. Ruitenberg, R. F. L. Vermeulen, R. N. Schouten, C. Abellán, W. Amaya, V. Pruneri, M. W. Mitchell, M. Markham, D. J. Twitchen, D. Elkouss, S. Wehner, T. H. Taminiau, and R. Hanson, Loophole-free Bell inequality violation using electron spins separated by 1.3 kilometres, *Nature* **526**, 682 (2015).

[4] C. M. Holland, Y. Lu, and L. W. Cheuk, On-demand entanglement of molecules in a reconfigurable optical tweezer array, *Science* **382**, 1143 (2023).

[5] T. Takayama, J. Chaloupka, A. Smerald, G. Khaliullin, and H. Takagi, Spin-Orbit-Entangled Electronic Phases in 4d and 5d Transition-Metal Compounds, *J. Phys. Soc. Jpn.* **90**, 062001 (2021).

[6] D. Gotfryd, E. M. Pärschke, J. Chaloupka, A. M. Oleś, and K. Wohlfeld, How spin-orbital entanglement depends on the spin-orbit coupling in a Mott insulator, *Phys. Rev. Research* **2**, 013353 (2020).

[7] A. S. Miñarro, M. Villa, B. Casals, S. Plana-Ruiz, F. Sánchez, J. Gázquez, and G. Hernanz, Spin-orbit entanglement driven by the Jahn-Teller effect, *Nat. Commun.* **15**, 8694 (2024).

[8] Z. Shen, S. Ding, A. Zhao, F. A. Evangelista, and Y. Wang, Witnessing Spin-Orbital Entanglement using Resonant Inelastic X-Ray Scattering, *arXiv:2512.06718v1 [quant-ph]* <https://doi.org/10.48550/arXiv.2512.06718> (2025).

[9] P. R. Anandan, M. Nadeem, C.-H. Lin, S. Singh, X. Guan, J. Kim, S. Shahrokhi, M. Z. Rahaman, X. Gen, J.-K. Huang, H. Nguyen, H. Hu, P. Sharma, J. Seidel, X. Wang, and T. Wu, Spin-orbital coupling in all-inorganic metal-halide perovskites: The hidden force that matters, *Appl. Phys. Rev.* **10**, 041312 (2023).

[10] G. Bussière, C. Reber, D. Neuhauser, D. A. Walter, and J. I. Zink, Molecular Properties Obtained by Analysis of Electronic Spectra Containing Interference Dips. Comparisons of Analytical Equations and Exact Models Based on Coupled Potential Energy Surfaces, *J. Phys. Chem. A* **107**, 1258 (2003).

[11] O. Maalej, O. Taktak, B. Boulard, and S. Kammoun, Study with Analytical Equations of Absorption Spectra Containing Interference Dips in Fluoride Glasses Doped with Cr³⁺, *J. Phys. Chem. B* **120**, 7538 (2016).

[12] D. Neuhauser, T.-J. Park, and J. I. Zink, Analytical Derivation of Interference Dips in Molecular Absorption Spectra: Molecular Properties and Relationships to Fano's Antiresonance, *Phys. Rev. Lett.* **85**, 5304 (2000).

[13] J. F. Pérez-Torres, Relativistic Effects in Ligand Field Theory (I): Optical Properties of d^1 Atoms in O_h' Symmetry, *Inorg. Chem.* **63**, 15016 (2024).

[14] J. L. Sanz-Vicario, J. F. Pérez-Torres, and G. Moreno-Polo, Electronic-nuclear entanglement in H_2^+ : Schmidt decomposition of non-Born-Oppenheimer wave functions expanded in nonorthogonal basis sets, *Phys. Rev. A* **96**, 022503 (2017).

[15] M. Blavier, R. D. Levine, and F. Remacle, Time evolution of entanglement of electrons and nuclei and partial traces in ultrafast photochemistry, *Phys. Chem. Chem. Phys.* **24**, 17516 (2022).

[16] G. Greene-Diniz, C. N. Self, M. Krompiec, L. Coopmans, M. Benedetti, D. M. noz Ramos, and M. Rosenkranz, Measuring correlation and entanglement between molecular orbitals on a trapped-ion quantum computer, *Sci. Rep.* **15**, 28409 (2025).

[17] J. F. P. Mosquera and J. L. Sanz-Vicario, Electronic-nuclear entanglement in Born-Oppenheimer wave functions and beyond, *J. Chem. Phys.* **164**, 064105 (2026).

[18] O. Taktak, H. Souissi, and S. Kammoun, Optical absorption properties of ZnF_2 - RO - TeO_2 ($R = Pb, Cd$ and Zn) glasses doped with chromium (III): Neuhauser model and crystal field study, *Optical Materials* **113**, 110682 (2021).

[19] H. Bethe, Termaufspaltung in Kristallen, *Annalen der Physik* **395**, 133 (1929).

[20] J. H. V. Vleck, Quantum Mechanics: The Key to Understanding Magnetism, *Science* **201**, 113 (1978).

[21] C. J. Ballhausen, *Introduction to Ligand Field Theory* (McGraw-Hill, New York, 1962).

[22] J. F. Pérez-Torres, Relativistic Effects in Ligand Field Theory (II): Optical and Magnetic Properties of d^1 Atoms in Cubic and Tetragonal Symmetries, *J. Phys. Chem. A* **129**, 3844 (2025).

[23] V. García-Rojas and J. F. Pérez-Torres, Quantifying the Spin-Orbital Entanglement in $5d^1$ Quantum Materials, *arXiv:2511.18046v1* [physics.chem-ph]

[24] A. J. Ceulemans, *Group Theory Applied to Chemistry* (Springer, Dordrecht, Heidelberg, New York and London, 2013).

[25] Y.-S. Dou, Equations for Calculating Dq and B , *J. Chem. Educ.* **67**, 134 (1990).

[26] T. Sugano, Y. Tanabe, and H. Kamimura, *Multiplets of Transition-Metals Ions in Crystals* (Academic Press, New York and London, 1970).

[27] A. Lempicki, L. Andrews, S. J. Nettel, B. C. McCollum, and E. I. Solomon, Spectroscopy of Cr^{3+} in Glasses: Fano Antiresonances and Vibronic "Lamb Shift", *Phys. Rev. Lett.* **44**, 1234 (1980).

[28] O. Villain, L. Galois, and G. Calas, Spectroscopic and structural properties of Cr^{3+} in silicate glasses: Cr^{3+} does not probe the average glass structure, *J. Non-Cryst. Solids* **356**, 2228 (2010).

[29] G. L. Stamokostas and G. A. Fiete, Mixing of $t_{2g} - e_g$ orbitals in $4d$ and $5d$ transition metal oxides, *Phys. Rev. B* **97**, 085150 (2018).

[30] W. C. Fernelius, J. E. Blanch, B. E. Bryant, K. Terada, R. S. Drago, and J. K. Stille, *Inorganic Syntheses* (McGraw-Hill, New York, Toronto, London, 1957) p. 130.

[31] V. García-Rojas and J. F. Pérez-Torres, Derivation of Dq/B and C/B from Electronic Spectra of Transition Metal Ions in Cubic Fields Using Auxiliary Tanabe-Sugano Diagrams, *J. Chem. Educ.* **100**, 251 (2023).

[32] S. Adachi, The Best Approximate Racah Parameter Ratios of $r = C/B$ for the Cr^{3+} -Activated Fluoride and Oxide Phosphors, *ECS J. Solid State Sci. Technol.* **14**, 086001 (2025).

[33] C. L. Kanth, B. V. Raghavaiah, B. A. Rao, and N. Veeriah, Spectroscopic investigations on ZnF_2 - MO - TeO_2 ($MO = ZnO, CdO$ and PbO) glasses doped with chromium ions, *J. Quant. Spectrosc. Radiat. Transfer* **90**, 97 (2005).

[34] L.-L. Sun, Y.-S. Song, and S. Yu, Entanglement detection beyond the local bound with coarsely calibrated measurements, *Phys. Rev. A* **113**, L010405 (2026).

[35] W. Greiner, *Relativistic Quantum Mechanics: Wave Equations*, 3rd ed. (Springer, Berlin, 2000).

<https://doi.org/10.48550/arXiv.2511.18046> (2025).